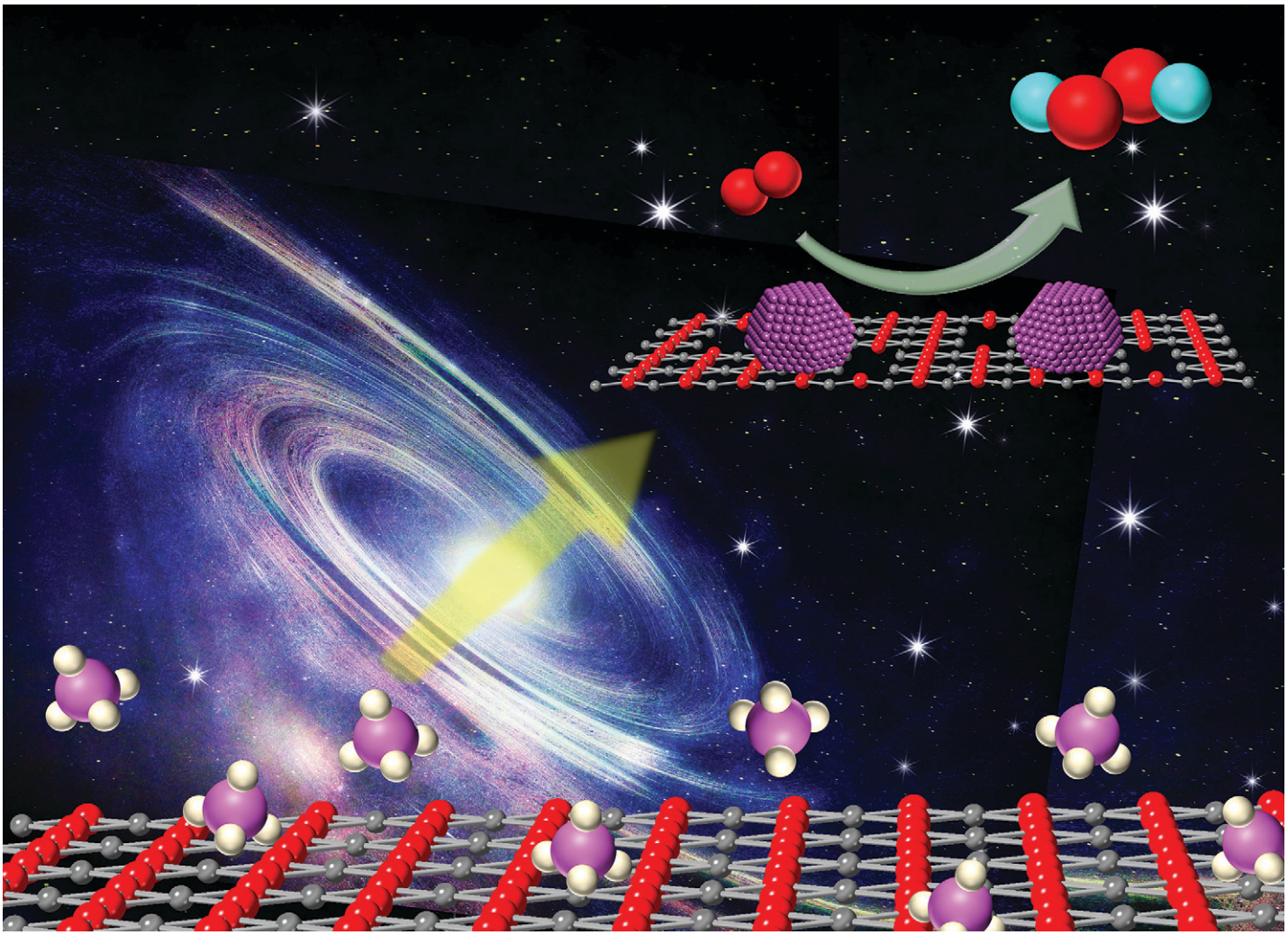

Showcasing the joint research by Professor Hiroaki Tada (Institutes of Innovation for Future Society, Nagaya University, Aichi, Japan), and Dr. Shin-ichi Naya and Dr. Miwako Teranishi (Environmental Research Laboratory, Kindai University, Osaka, Japan).

Facile preparation of highly active zirconia-supported gold nanoparticle catalyst

Au nanoparticle-loaded zirconia prepared by a modified DP method with a pre-step of long-time stirring of ZrO_2 nanoparticles in $HAuCl_4$ solution (Au/ZrO_2-MDP) exhibits an extraordinarily high catalytic activity for H_2O_2 production by $2e^-$-ORR using HCOOH. Regardless of the insulating character of ZrO_2, the turnover frequency (TOF) of Au/ZrO_2-MDP is much exceeding those of various Au/n-type semiconducting metal oxides.

As featured in:

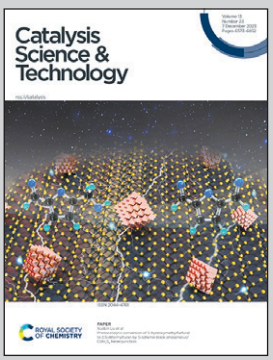

See Shin-ichi Naya, Hiroaki Tada *et al.*, *Catal. Sci. Technol.*, 2023, **13**, 6662.

ROYAL SOCIETY OF CHEMISTRY

rsc.li/catalysis

Registered charity number: 207890

Catalysis Science & Technology

ROYAL SOCIETY OF CHEMISTRY

PAPER

View Article Online
View Journal | View Issue

Cite this: *Catal. Sci. Technol.*, 2023, 13, 6662

Facile preparation of highly active zirconia-supported gold nanoparticle catalyst†

Shin-ichi Naya,*[a] Miwako Teranishi[a] and Hiroaki Tada *[b]

Received 17th May 2023,
Accepted 18th August 2023

DOI: 10.1039/d3cy00689a

rsc.li/catalysis

Efficient production of hydrogen peroxide (H_2O_2) from oxygen (O_2) is an important research topic in chemistry. Au nanoparticles loaded on n-type semiconducting metal oxides by the deposition precipitation (DP) method (Au/n-MOs) are known to possess catalytic activity for two electron-oxygen reduction reaction. In this study, zirconia-supported Au nanoparticles (NPs) were prepared by the usual DP method (Au/ZrO_2-DP) and a modified DP method with a pre-step of long-term stirring of ZrO_2 NPs in $HAuCl_4$ solution (Au/ZrO_2-MDP). Regardless of the insulating character of ZrO_2, Au/ZrO_2-MDP stably yields H_2O_2 from O_2 and HCOOH at 25 °C with a turnover frequency (TOF) of 1.0×10^2 h^{-1} and selectivity of 97%. The TOF is much larger than the values of Au/ZrO_2-DP and various Au/n-MOs. Spectroscopic measurements indicated that the unexpectedly high catalytic activity of Au/ZrO_2-MDP can be induced by effective introduction of O-vacancies to the ZrO_2 surface.

Introduction

Metal oxide-supported Au nanoparticles (NPs) smaller than 10 nm are known to exhibit high catalytic activity for various important reactions including CO oxidation, alcohol oxidation, hydrogen evolution, hydrogenation, and C–C coupling, while bulk Au is chemically inactive.[1–4] The catalytic activity strongly depends on the kind of the metal oxide supports as well as the Au particle size. Among them, n-type semiconducting metal oxides such as TiO_2 and CeO_2 are most widely used as the support for Au NPs (Au/n-MOs).[3,4] A positive correlation was previously recognized between the catalytic activity of Au/n-MOs for alcohol oxidation and the conduction band (CB) minimum of n-MOs.[5] Also, Au/n-$MTiO_3$ (M = Ca, Sr, Ba) with high CB minimum has recently been reported to show high catalytic activity for H_2O_2 production from O_2 with formic acid (HCOOH) as a proton and electron donor at ambient temperature and pressure (eqn (1)).[6] HCOOH with hydrogen storage capacity of 4.3 wt% and normal boiling point of 374 K can be a highly promising hydrogen storage and carrier material.[7,8] HCOOH is one of major products from non-edible biomass,[9] while it has recently been synthesized from H_2 and CO_2 using an iridium catalyst under mild conditions.[10] Thus, the process (eqn (1)) can be regarded as a green and sustainable process for H_2O_2 production.

$$O_2 + HCOOH \rightarrow H_2O_2 + CO_2 \quad (1)$$

On the other hand, insulating ZrO_2-supported Au NPs (Au/ZrO_2) were reported to show catalytic activity for CO oxidation,[11] although the activity is much lower than Au/TiO_2.[12] The significant catalytic activity of Au/ZrO_2 can originate from the oxygen vacancy at the Au–ZrO_2 interface.[13] In usual, catalytically active Au/MOs are conveniently prepared by the deposition precipitation (DP) process consisting of neutralization of $HAuCl_4$ solution (step 1), adsorption of the resulting $[Au(OH)_3Cl]^-$ complex on MO (step 2), and Au NP formation by heating in the air (step 3).[14]

While repeating the preparation of Au/ZrO_2 catalysts by the DP method, we have found that a highly active Au/ZrO_2 catalyst can be obtained by stirring the ZrO_2 particle-dispersed $HAuCl_4$ solution for a long period of time. Here we present the simple modified DP method for the preparation of Au/ZrO_2 (Au/ZrO_2-MDP). As a test reaction, Au/MO-catalyzed production of H_2O_2 from O_2 and HCOOH (eqn (1)) was carried out. Au/ZrO_2-MDP prepared at heating temperature = 400 °C has been shown to exhibit an extraordinarily high catalytic activity for H_2O_2 production.

Results and discussion

Catalyst preparation and characterization

Commercial non-faceted monoclinic ZrO_2 particles (mean particle size = 20 nm, specific surface area = 100 m^2 g^{-1} UEP-100, Daiichi Kigenso Kagaku Kogyo Co.) were used as the

[a] *Environmental Research Laboratory, Kindai University, 3-4-1, Kowakae, Higashi-Osaka, Osaka 577-8502, Japan. E-mail: shinichi.naya@itp.kindai.ac.jp*
[b] *Institutes of Innovation for Future Society, Nagoya University, Furo-cho, Chikusa-ku, Nagoya 464-8603, Japan. E-mail: hiroaki.tada@mirai.nagoya-u.ac.jp*

† Electronic supplementary information (ESI) available. See DOI: https://doi.org/10.1039/d3cy00689a

support of Au NPs. In the normal DP method, just after adding ZrO_2 particles into $HAuCl_4$ aqueous solution, the suspension was neutralized to pH 7.0, and the suspension was stirred at 80 °C for 2 h. The resulting particles were washed and dried, and calcined 1 h. In the present modified DP method, ZrO_2 particles were added to the $HAuCl_4$ solution, and then, the suspension was stirred at 25 °C for 24 h. Subsequent application of the same procedures as the normal DP method yielded Au/ZrO_2. The samples prepared by the normal and modified DP methods at heating temperature t_c (°C) are designated as Au/ZrO_2-DP_{t_c} and Au/ZrO_2-MDP_{t_c}, respectively. The Au loading amounts of Au/ZrO_2-DP and Au/ZrO_2-MDP are quantified to be 0.69 mass% and 0.67 mass%, respectively, by inductively coupled plasma spectroscopy. In the XRD patterns of ZrO_2, Au/ZrO_2-DP_{400}, and Au/ZrO_2-MDP_{400} (Fig. S1†), the diffraction peaks are observed at 2θ = 28.2°, 31.5°, and 50.1° due to the diffraction from the (−111), (111), and (−220) planes for the monoclinic ZrO_2 (ICDD No 00-036-0420), respectively. No diffraction of Au is observed for Au/ZrO_2-DP and Au/ZrO_2-MDP because of the small loading amount. Fig. 1a shows the high resolution-transmission electron microscopic (HR-TEM) image of Au/ZrO_2-MDP_{400}. The *d*-spacings of the deposit and support are in agreement with the values of Au(111) and monoclinic ZrO_2(011) planes, respectively. Fig. 1b shows Kubelka–Munk transformed UV-vis-NIR absorption spectra for ZrO_2, Au/ZrO_2-DP_{400}, and Au/ZrO_2-MDP_{400}. Unmodified ZrO_2 only has the interband-transition absorption at wavelength (λ) < 240 nm. In the absorption spectra of Au/ZrO_2-DP_{400} and Au/ZrO_2-MDP_{400}, new absorption appears around 550 nm due to the localized surface plasmon resonance (LSPR) of Au NPs. Fig. 1c and the inset show the TEM image and Au particle size distribution of Au/ZrO_2-MDP_{400}, respectively, and the data on Au/ZrO_2-DP_{400} are provided in ESI† (Fig. S2). Au NPs with a mean particle size (d_{Au}) = 3.6 ± 0.5 nm for Au/ZrO_2-MDP_{400} and d_{Au}= 4.6 ± 0.7 nm for Au/ZrO_2-DP_{400} are deposited on the ZrO_2 surface. Fig. 1d shows high-angle annular dark field scanning TEM (HAADF-STEM) image of Au/ZrO_2-MDP_{400}. It can be seen more clearly that the Au NPs shown by the bright spots are highly dispersed on the ZnO surface. Previously, the formation of noble metal (core)–metal oxides (shell) NPs (M@MOs) such as Ru@SnO_2 was previously reported during a reduction–oxidation process through the strong metal support interaction,[15] but no such particle is observed in the present Au/ZrO_2 systems (Fig. S3†). The similar absorption spectra of Au/ZrO_2-DP_{400} and Au/ZrO_2-MDP_{400} also indicate that the loading amount, size, and shape of Au NPs are comparable each other.

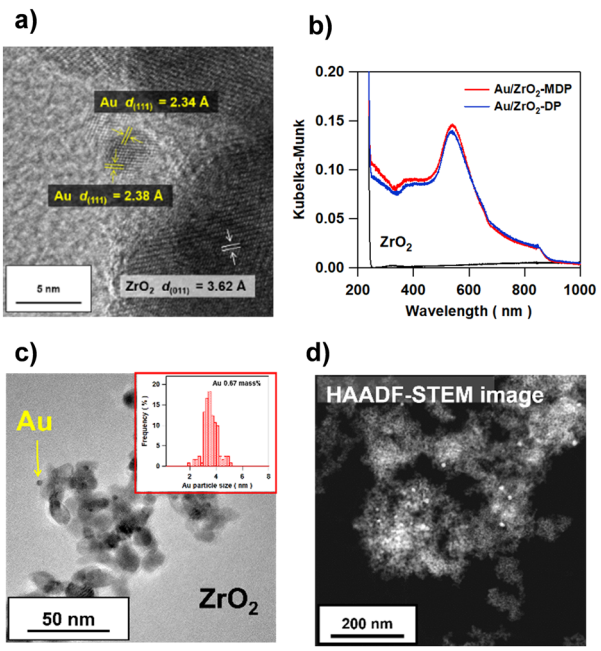

Fig. 1 (a) HR-TEM image of Au/ZrO_2-MDP_{400}. (b) Kubelka–Munk-transformed UV-vis-NIR absorption spectra of ZrO_2, Au/ZrO_2-DP_{400}, and Au/ZrO_2-MDP_{400}. (c) TEM image of Au/ZrO_2-MDP_{400}. The inset shows the Au particle size distribution. (d) HAADF-STEM image of Au/ZrO_2-MDP_{400}.

Catalytic H_2O_2 production and stability test

The catalytic activities of Au/ZrO_2 and various Au/n-MOs for H_2O_2 production from aerated 1.06 M aqueous solution of HCOOH (eqn (1)) were evaluated at 25 °C. The concentration of H_2O_2 was quantified by the iodometric titration.[16] Fig. 2a shows time courses for H_2O_2 generation in the ZrO_2, Au/ZrO_2-DP_{400}, Au/ZrO_2-MDP_{400} systems, and the Au/TiO_2 system

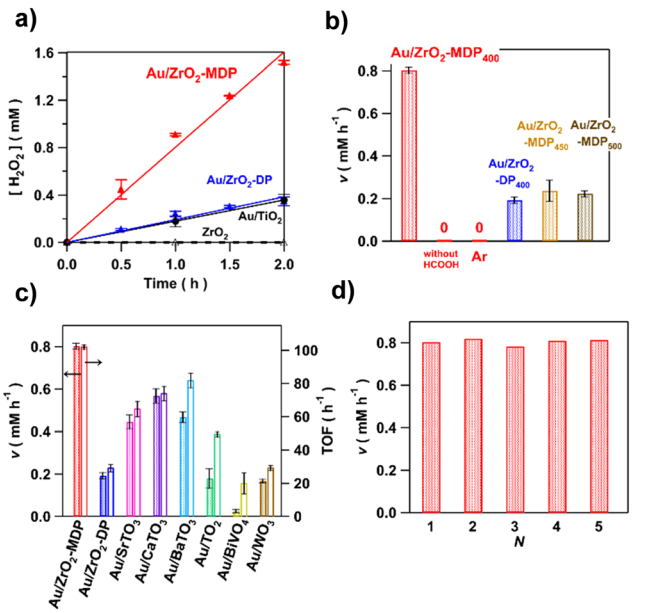

Fig. 2 (a) Time courses for the H_2O_2 generation in the systems of ZrO_2, Au/ZrO_2-DP_{400}, Au/ZrO_2-MDP_{400}, and Au/TiO_2 in aerated HCOOH aqueous solution at 25 °C. (b) Rate of H_2O_2 generation (*v*) in the Au/ZrO_2 systems under the same conditions, and controlled conditions without O_2 or HCOOH. (c) Comparison of the catalytic activities (*v* and TOF) of Au/ZrO_2-DP_{400} and Au/ZrO_2-MDP_{400} with those of various Au/n-MOs. (d) Repeated reactions in aerated HCOOH aqueous solution at 25 °C using the same Au/ZrO_2-MDP_{400} catalyst.

as a typical Au/n-MO for comparison. While unmodified ZrO_2 is inactive, every Au/MO system shows catalytic activity for the generation of H_2O_2 whose amount increases almost in proportion to reaction time. Fig. 2b shows the rate of H_2O_2 generation (v) in each system. Au/ZrO_2-DP_{400} provides a v value of 0.19 mM h^{-1} comparable with that of Au/TiO_2 (0.18 mM h^{-1}). The rate of reaction in the Au/ZrO_2-MDP_{400} system (0.80 mM h^{-1}) is 4.2-fold greater than that of the Au/ZrO_2-DP_{400} system. Fig. 2c compares the v values and turnover frequencies (TOFs) of Au/ZrO_2-DP_{400} and Au/ZrO_2-MDP_{400} with those of various Au/n-MOs. The TOF was calculated by assuming that the surface Au atoms are catalytically active sites to compare the values previously reported for various Au/MOs (Table S1†). The surface Au atoms were calculated by the d_{Au} and the dispersion.[17] Surprisingly, Au/ZrO_2-MDP_{400} exhibits the highest catalytic activity among the Au/MOs, and the TOF reaches 1.0×10^2 h^{-1}. The analysis by gas chromatography confirmed the evolution of CO_2, and HCOOH utilization efficiency (η) defined by eqn (2) reaches 97% (Fig. S4†).

$$\eta\ (\%) = (\text{mole number of } H_2O_2/\text{mole number } CO_2) \times 100 \quad (2)$$

To check the stability of Au/ZrO_2-MDP, the reaction was repeated 5 times using the same Au/ZrO_2-MDP_{400}. As shown in Fig. 2d, no decay in the catalytic activity is observed. Further, the characterization by means of XRD, TEM, and XP spectra also confirm that the structure and electronic state of Au/ZrO_2-MDP are maintained after the repeated reactions (Fig. S5†). Clearly, the introduction of the long-time stirring of ZrO_2 particles in the $HAuCl_4$ solution to the DP process as a pre-step remarkably enhances the catalytic activity of Au/ZrO_2 for two electron-oxygen reduction reaction ($2e^-$-ORR).

Activation mechanism

The catalytic activity of Au NPs is well known to strongly depend on the size and shape.[3,4] On the other hand, the LSPR-peak wavelength of Au NPs is sensitive to the size and shape of Au NP. The similar absorption spectra of Au/ZrO_2-DP and Au/ZrO_2-MDP suggest that the size and shape of Au NPs are not the main factors causing the large difference in their catalytic activities.

To gain the insight into the origin for the outstanding catalytic activity of Au/ZrO_2-MDP_{400}, firstly, the change in the state of the samples during step 2 to step 3 in the DP and MDP processes were traced by thermal analysis for the Au complex-adsorbed on ZrO_2 (Au^{3+}/ZrO_2). Fig. 3a shows thermogravimetry (TG)-differential thermal analysis (DTA) curves for Au^{3+}/ZrO_2-DP and Au^{3+}/ZrO_2-MDP in the air. In each DTA curve, an endothermic peak due to the desorption of physically adsorbed H_2O is observed around 100 °C with several exothermic peaks in the range from 200 °C to 300 °C. The latter peaks are ascribable to the decomposition of the adsorbed Au^{3+}-complex yielding Au NP since the absorption due to the LSPR characteristic of Au NPs appears at $t_c \gtrsim 350$ °C (Fig. S6†). Noticeably, an additional exothermic peak is present at 450 °C only in the DTA curve for Au^{3+}/ZrO_2-MDP. Then, Au/ZrO_2-MDP samples were prepared at 450 °C and 500 °C, and the catalytic activity for H_2O_2 generation from aerated HCOOH solution was examined. As shown in Fig. 2b, the catalytic activity is greatly reduced at $t_c \geq 450$ °C to be comparable with that of Au/ZrO_2-DP_{400}.

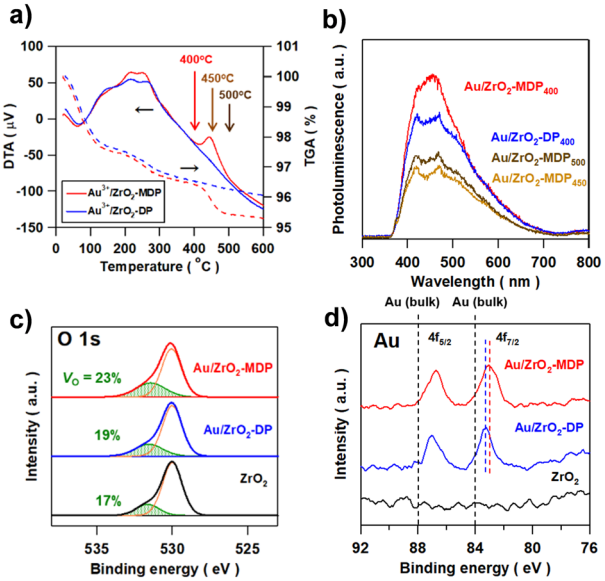

Fig. 3 (a) TG (broken lines)-DTA (solid lines) curves for Au^{3+}/ZrO_2-MDP (red) and Au^{3+}/ZrO_2-DP (blue). (b) PL spectra of Au/ZrO_2-$MDP_{400,450,500}$ and Au/ZrO_2-DP_{400} measured at l_{ex} = 280 nm at 77 K. (c) O 1s-XP spectra of Au/ZrO_2-MDP_{400}, Au/ZrO_2-DP_{400}, and ZrO_2. (d) Au 4f-XPS spectra for Au/ZrO_2-MDP_{400}, Au/ZrO_2-DP_{400}, and ZrO_2.

Secondly, photoluminescence (PL) spectra of Au/ZrO_2-$MDP_{400,450,500}$ and Au/ZrO_2-DP_{400} were measured at excitation wavelength (λ_{ex}) = 280 nm at 77 K. Every sample has a broad emission band around 480 nm due to the O-vacancies in ZrO_2.[18,19] The emission of Au/ZrO_2-MDP_{400} is significantly stronger than that of Au/ZrO_2-DP_{400}. The emission intensity of Au/ZrO_2-MDP steeply decreases at $t_c \geq 450$ °C. These results indicate that Au/ZrO_2-DP_{400} has more O-vacancies than the other samples. Thirdly, X-ray photoelectron (XP) spectra of Au/ZrO_2-MDP_{400}, Au/ZrO_2-DP_{400}, and ZrO_2 were measured. No discernable difference is observed between the Zr3d-XP spectra (Fig. S7†). In Fig. 3c, each O1s-XP spectrum can be deconvoluted into two signals with the binding energies (E_B) of 530. 2 eV (S1) and 532.0 eV (S2) assignable to the lattice O and the lattice oxygen associated with in the oxygen deficient region (or surface OH groups), respectively.[20] The S2-signal percentage calculated from {area(S2)/area(S1) + area(S2)} × 100 increases in the order of ZrO_2 (17%) < Au/ZrO_2-DP (19%) < Au/ZrO_2-MDP (23%), which is also consistent with the conclusion drawn from the PL data. On the other hand, bulk Au possesses two signals at E_B = 84.0 eV and 87.7 eV due to the emission from the $Au4f_{7/2}$ and $Au4f_{5/2}$ orbitals, respectively.[21] In Fig. 3d, the signals of Au/ZrO_2-DP_{400} and Au/ZrO_2-MDP_{400} shift towards the lower energy

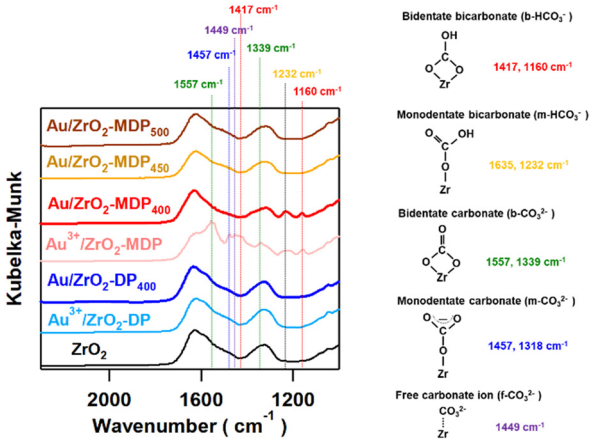

Fig. 4 DRIFT spectra for Au^{3+}/ZrO_2 (MDP and DP) before calcined, Au/ZrO_2 (MDP and DP) with the calcination at t_c = 400 °C, 450 °C, and 500 °C, and ZrO_2 for comparison.

side, and the E_B shift in the Au/ZrO_2-MDP_{400} system (ΔE_B, $Au4f_{7/2}$ = −0.9 eV) is more pronounced than the Au/ZrO_2-DP_{400} system (ΔE_B, $Au4f_{7/2}$ = −0.7 eV). Evidently, O-vacancies are effectively introduced into the ZrO_2 surface by the MDP process simultaneously with the excessive electrons transferred to Au NPs.

Further, the mechanism on the introduction of O-vacancy into the ZrO_2 support of Au/ZrO_2-MDP_{400} was studied by means of diffuse reflectance Fourier-transformed infrared (DRIFT) spectroscopy. Most Au complexes probably exist as $[HAu(OH)_3Cl]^-$ at pH ~7.[22] $[HAu(OH)_3Cl]^-$ complex is adsorbed on ZrO_2 *via* the ligand exchange between Cl^- and surface hydroxy groups (Zr_s–OH).[23] Fig. 4 shows the DRIFT spectra for Au^{3+}/ZrO_2-MDP before and after calcination at t_c = 400 °C, 450 °C, and 500 °C, and for comparison, ZrO_2 and Au/ZrO_2-DP_{400}. While these spectra are similar, a closer inspection indicates the presence of the absorption at 1232 cm^{-1} and 1160 cm^{-1} only in the spectra of Au^{3+}/ZrO_2-MDP and Au/ZrO_2-MDP_{400}. The former and latter signals can be assigned to the adsorbed monodentate carbonate and bidentate carbonate, respectively,[24–26] disappearing at $t_c \geq$ 450 °C. Thus, the exothermic peak around 450 °C in the Au^{3+}/ZrO_2-MDP (Fig. 3a) results from the decomposition of the adsorbed carbonates. Recent temperature programed desorption measurements have shown that the decomposition of carbonate on Au/ZrO_2 occurs at 450 °C with the dehydration of surface hydroxy groups.[27,28]

In the MDP process (Scheme 1), the long-time stirring of the suspension of ZrO_2 particles in acidic $HAuCl_4$ solution causes the hydrolysis of the ZrO_2 surface to form Zr_s–OH groups and O-vacancies, where the subscript s denotes the surface atom. During the neutralization, CO_2 is dissolved into the ZrO_2 suspension to be adsorbed on the surface as carbonates with the chemisorption of $[Au(OH)_3Cl]^-$ complexes. Upon heating at t_c = 400 °C, the adsorbed Au^{3+} complexes are transformed to Au NPs, while the surface carbonates and oxygen vacancies remain. At $t_c \geq$ 450 °C, the carbonates are decomposed into CO_2 with the partial disappearance of surface O-vacancies.

These results above strongly suggest that the effective introduction of O-vacancies to the ZrO_2 surface by the MDP process is deeply associated with the high catalytic activity of Au/ZrO_2-MDP for $2e^-$-ORR by HCOOH. Recently, Au/ZrO_2 prepared by a colloidal deposition method has been reported to exhibit catalytic activity for CO oxidation although it is significantly lower than that of Au/TiO_2.[12] The authors have revealed by the temporal analysis of products technique that the CO oxidation on Au/TiO_2 at 80 °C and higher proceeds *via* the Au-assisted Mars–van Krevelen mechanism where CO is oxidized by the lattice O on the TiO_2 surface to be reproduced by O_2.[29] Also, recent first principle calculations

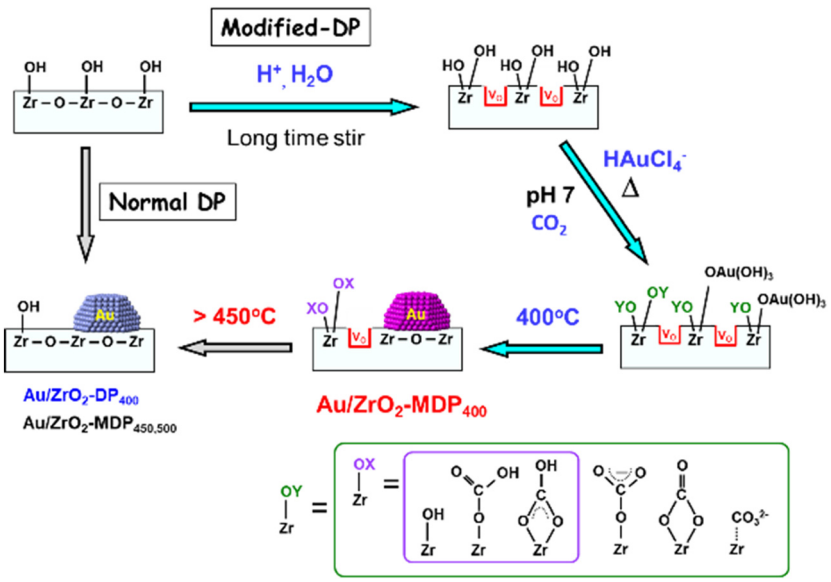

Scheme 1 Proposed activation mechanism on the DP method for the preparation of Au/ZrO_2.

have indicated that the Au/ZrO_2-catalyzed CO oxidation can also proceed *via* the same mechanism.[13,30] Importantly, these studies have pointed out the significance of O-vacancies on the surface of the MO support for the activation of O_2. However, the Au-assisted Mars–van Krevelen mechanism would be excluded from the possible mechanisms in this $2e^-$-ORR because the O–O bond of O_2 is maintained and the reaction temperature is 25 °C.[31] Meantime, the electron-richness of the MO-supported Au NPs can be one of the controlling factors of the catalytic activity for $2e^-$-ORR.[32,33] Consequently, the outstanding catalytic activity of Au/ZrO_2-MDP_{400} for $2e^-$-ORR may stem from fine tuning of the electronic state of Au NPs on ZrO_2 with the effective introduction of O-vacancies to the support surface (Fig. 3d). However, there is the possibility that oxygen defect sites around the perimeter interface of Au nanoparticles with ZrO_2 work catalytically active sites, and in this case, the TOF values will be even larger (Table S1†). Further work is needed to clarify the catalytically active sites at the atomic level to elucidate the detailed action mechanism.

Conclusions

We have presented a modified DP method with a pre-step of long-time stirring of ZrO_2 particles in $HAuCl_4$ solution for the preparation of Au/ZrO_2 (Au/ZrO_2-MDP). The sample prepared at heating temperature of 400 °C (Au/ZrO_2-MDP_{400}) has been found to exhibit an extraordinarily high catalytic activity for $2e^-$-ORR by HCOOH much exceeding those of various Au/n-MOs. Spectroscopic experiments indicated that the catalytic activity of Au/ZrO_2-MDP_{400} can be induced by effective introduction of O-vacancies to the ZrO_2 surface. Historically, the discovery of the catalytic activity of Au NPs and the subsequent remarkable progress in the application to various chemical reactions owe much to the development of the DP methods. Thus, we anticipate that the present modified DP method can contribute to further advance in this field.

Data availability

The data supporting the findings can be found in the article and ESI,† and are available from the authors upon reasonable request.

Author contributions

S. N. and M. T. conducted catalysts synthesis, characterization, and catalytic reaction experiments, and H. T. supervised the work and data analysis.

Conflicts of interest

There are no conflicts to declare.

Acknowledgements

This work was financially supported by JSPS KAKENHI Grant-in-Aid for Scientific Research (C) no. 20K05674 and 21K05236, the Futaba Foundation, Nippon Sheet Glass Foundation for Materials Science and Engineering, Sumitomo Foundation, Takahashi Industrial and Economic Research Foundation, and Kato Foundation for Promotion of Science.

Notes and references

1 Q.-Y. Bi, X.-L. Du, Y.-M. Liu, Y. Cao, H.-Y. He and K.-N. Fan, *J. Am. Chem. Soc.*, 2012, **134**, 8926–8933.
2 X. Liu, L. He, Y.-M. Liu and Y. Cao, *Acc. Chem. Res.*, 2014, **47**, 793–804.
3 T. Ishida, T. Maruyama, A. Taketoshi and M. Haruta, *Chem. Rev.*, 2020, **120**, 464–525.
4 M. Sankar, Q. He, R. V. Engel, M. A. Sainna, A. J. Logsdail, A. Roldan, D. J. Willock, N. Agarwal, C. J. Kiely and G. J. Hutchings, *Chem. Rev.*, 2020, **120**, 3890–3938.
5 S. Naya, M. Teranishi, R. Aoki and H. Tada, *J. Phys. Chem. C*, 2016, **120**, 12440–12445.
6 M. Teranishi, S. Naya and H. Tada, *J. Phys. Chem. C*, 2019, **123**, 9831–9837.
7 M. Grasemann and G. Laurenczy, *Energy Environ. Sci.*, 2012, **5**, 8171–8181.
8 X. Liu, L. He, Y.-M. Liu and Y. Cao, *Acc. Chem. Res.*, 2014, **47**, 793–804.
9 A. Boddien, B. Loges, F. Gaertner, C. Torborg, K. Fumino, H. Junge, R. Ludwig and M. Beller, *J. Am. Chem. Soc.*, 2010, **132**, 8924–8934.
10 J. F. Hull, Y. Himeda, W.-H. Wang, B. Hashiguchi, R. Periana, D. J. Szalda, J. T. Muckerman and E. Fujita, *Nat. Chem.*, 2012, **4**, 383–388.
11 X. Zhang, H. Wang and B. Xu, *J. Phys. Chem. B*, 2005, **109**, 9678–9683.
12 D. Widmann, Y. Lin, F. Schűth and R. J. Behm, *J. Catal.*, 2010, **276**, 292–305.
13 P. Schlexer, A. Ruiz Puigdollers and G. Paccioni, *Top. Catal.*, 2019, **62**, 1192–1201.
14 S. Tsubota, M. Haruta, T. Kobayashi, A. Ueda and Y. Nakahara, *Preparation of Catalysis V*, Elsevier, Amsterdam, 1991.
15 T. Mitsui, K. Tsutsui, T. Matsui, R. Kikuchi and K. Eguchi, *Appl. Catal., B*, 2008, **81**, 56–63.
16 R. Cai, Y. Kubota and A. Fujishima, *J. Catal.*, 2003, **219**, 214–218.
17 G. A. Somorjai, *Introduction to Surface Chemistry and Catalysis*, John Wiley & Sons, New York, 1994.
18 T. V. Perevalov, D. V. Gulyaev, V. S. Aliev, K. S. Zhuravlev, V. A. Gritsenko and A. P. Yelisseyev, *J. Appl. Phys.*, 2014, **116**, 244109.
19 C. Lin, C. Zhang and J. Lin, *J. Phys. Chem. C*, 2007, **111**, 3300–3307.
20 S. R. Teeparthi, E. W. Awin and R. Kumar, *Sci. Rep.*, 2018, **8**, 5541.

21 K. Tanaka, S. Tanuma, K. Dohmae, Y. Nagoshi and A. A. Nisawa, *X-Ray Photoelectron Spectroscopy*, ed. T. Sawada, S. Tanuma and K. Tanaka, Maruzen, Tokyo, 1998.
22 F. Moreau, G. C. Bond and A. O. Taylor, *J. Catal.*, 2005, **231**, 105–114.
23 G. C. Bond, C. Loius and D. T. Thompson, *Catalysis by Gold*, Imperial Collage Press, London, 2006.
24 K. Pokrovski, K. T. Jung and A. T. Bell, *Langmuir*, 2001, **17**, 4297–4303.
25 J. Li, J. Chen, W. Song, J. Liu and W. Shen, *Appl. Catal., A*, 2008, **334**, 321–329.
26 H. Takano, Y. Kirihata, K. Izumiya, N. Kumagai, H. Habazaki and K. Hashimoto, *Appl. Surf. Sci.*, 2016, **388**, 653–663.
27 X. Zhang, H. Shi and B.-Q. Xu, *J. Catal.*, 2011, **279**, 75–87.
28 Q.-Y. Bi, J.-D. Lin, Y.-M. Liu, H.-Y. He and F.-Q. Huang, *J. Power Sources*, 2016, **327**, 463–471.
29 D. Widmann and R. J. Behm, *Angew. Chem., Int. Ed.*, 2011, **50**, 10241–10245.
30 A. R. Puigdollers, P. Schlexer, S. Tosoni and G. Pacchioni, *ACS Catal.*, 2017, **7**, 6493–6513.
31 D. K. Widmann, A. Krautsieder, P. Walther, A. Brűckner and R. J. Behm, *ACS Catal.*, 2016, **6**, 5005–5011.
32 M. Teranishi, S. Naya and H. Tada, *J. Am. Chem. Soc.*, 2010, **132**, 7850–7851.
33 H. Kobayashi, M. Teranishi, R. Negishi, S. Naya and H. Tada, *J. Phys. Chem. Lett.*, 2016, **7**, 5002–5007.